Article

Predictive Model for Site-Selective Aryl and Heteroaryl C–H Functionalization via Organic Photoredox Catalysis

Kaila A. Margrey, Joshua B. McManus, Simone Bonazzi, Frederic Zecri, and David A Nicewicz

J. Am. Chem. Soc., **Just Accepted Manuscript** • DOI: 10.1021/jacs.7b06715 • Publication Date (Web): 18 Jul 2017

Predictive Model for Site-Selective Aryl and Heteroaryl C–H Functionalization via Organic Photoredox Catalysis

Kaila A. Margrey,[†] Joshua B. McManus,[†] Simone Bonazzi,[‡] Frederic Zecri[‡] and David A. Nicewicz[†*]

[†]Department of Chemistry, University of North Carolina at Chapel Hill, Chapel Hill, North Carolina, 27599-3290, United States

[‡]Novartis Institutes for Biomedical Research, Global Discovery Chemistry, 181 Massachusetts Avenue, Cambridge, MA 02139, United States

Supporting Information Placeholder

ABSTRACT: Direct C–H functionalization of aromatic compounds is a useful synthetic strategy that has garnered much attention due to its application to pharmaceuticals, agrochemicals, and late stage functionalization reactions on complex molecules. Based on previous methods disclosed by our lab, we sought to develop a predictive model for site selectivity and extend this aryl functionalization chemistry to a selected set of heteroaromatic systems commonly used in the pharmaceutical industry. Using electron density calculations, we were able to predict site selectivity of direct C–H functionalization in a number of heterocycles and identify general trends observed across heterocycle classes.

INTRODUCTION

The selective functionalization of carbon-hydrogen bonds via catalytic methodologies represents a powerful approach for streamlining the construction of complex molecules. Moreover, the direct functionalization of aryl C–H bonds to C–C, C–O, C–N or C–F bonds is a strategy that has found widespread application in the late-stage derivatization of medicinal agents.[1] While this approach is powerful for diverse late-stage target modifications, predicting of the site of functionalization can often be challenging.[2,3,4,5,6]

To circumvent this obstacle, computational models have been developed alongside other C–H functionalization methodologies to better predict the sites most likely to undergo reactivity for a given system. White and co-workers have developed a catalyst-controlled aliphatic C–H oxidation methodology and included a predictive model that correlates the physical properties of a given substrate and the observed experimental site of functionalization.[7] Similarly, the Baran and Blackmond groups pioneered a radical-based C–H functionalization of electron-deficient heteroarenes and systematically investigated a number of parameters that affected regioselectivity, reporting general trends observed through experimental reactivity as their model.[8] Sigman and Davies disclosed a mathematical model for a rhodium-catalyzed C–H insertion derived from computationally-predicted infrared vibrations of a diazo ester starting material and natural bond orbital (NBO) point charges of substrates.[9] These predictive models are important for extending reaction development to late-stage derivatization, where site selectivity can be more difficult to determine *a priori*.

Our lab previously reported a site-selective arene C–H amination via an organic photoredox-based catalyst system, consisting of an acridinium catalyst and a nitroxyl radical cocatalyst.[10] We were able to demonstrate the addition of several nitrogen heterocycles to a variety of electron-rich aromatic systems in good to excellent yields. In most examples with monosubstituted aromatic substrates, good selectivity for the *para* over the *ortho* regioisomer was observed, and for several disubstituted benzenes and aromatic heterocycles, only one product was detected. This methodology was also applied to several complex substrates, affording single regioisomers with pyrazole as the azole coupling partner. We also demonstrated the addition of ammonia to electron-rich arenes using ammonium salts to afford anilines in good yields and modest regioselectivities. More recently, we have disclosed a strategy for aryl C–H cyanation, also relying on aryl cation radical intermediates.[11]

Data from our previous work are consistent with the reaction proceeding through the visible light-mediated (455 nm blue LEDs) excitation of the acridinium photoredox catalyst, which undergoes single electron transfer (SET) from the arene to generate an aryl cation radical (Figure 1). Nucleophilic addition to this species followed by deprotonation leads to a cyclohexadienyl radical intermediate, which rearomatizes to afford the desired product. The aerobic conditions facilitate catalyst turnover[12,13] and assist in the aromatization.

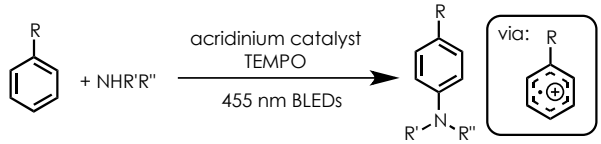

Figure 1. General reaction for photoredox-mediated aryl amination.

This system demonstrates a strong proclivity toward *para* functionalization for benzenoid substrates. However, when heteroaromatic or fused aromatic substrates are used, anticipating the site selectivity is nontrivial. Consequently, we aimed to develop a predictive model for use with aromatic heterocycles commonly present in biologically active compounds to identify the site most likely to undergo functionalization. Herein, we report the development of a simple computational model to predict reactivity and regioselectivity based on several innate factors of the aromatic system: (i) oxidation of the aromatic substrate by an acridinium

photocatalyst based on redox potentials; (ii) the electrophilicity of the resultant aryl cation radical after single electron oxidation; (iii) the representation of the cation radical intermediate as a delocalized or a localized distonic alkene cation radical; (iv) the change in electron density between the neutral arene and the corresponding cation radical; and (v) the electronic nature and position of substituents.

Computational Approaches to Arene Redox Potentials and Site Selectivity

Important for predicting reactivity is the determination of substrate redox potentials. While oxidation potentials for many common aromatic and heteroaromatic systems have been reported, acquiring redox potentials requires access to a potentiostat, which may be uncommon in most synthetic laboratories. To circumvent the need for electrochemical instrumentation, our laboratory previously disclosed a computational method to predict single electron redox potentials, and the calculated values of over 180 compounds correlate strongly to experimental values.[17] This approach can be utilized to determine the feasibility for arene oxidation by the photooxidation catalyst. Based on prior work, we elected to use di-*tert*-butyl-*N*-Ph-mesityl-acridinium tetrafluoroborate as the catalyst (**1**) since higher yields are generally observed with this derivative ($E_{1/2}$ ($Cat^{*}/Cat^{\bullet}$) $\leq$ +2.15V vs. SCE).[10] Thus, we anticipated that arenes with calculated oxidation potentials $E_{calc,ox}$ ($arene^{\bullet+}$/arene) $\leq$ +2.15V vs. SCE would be in range for oxidation by this photocatalyst.

Site selectivity for polar arene reactivity modes such as electrophilic aromatic substitution (E_AS) and nucleophilic aromatic substitution (S_NAr) can be predicted based on preexisting directing groups. Electrophilic aromatic substitution employs electron-rich arenes as nucleophiles, with reactivity generally occurring at positions *para* and *ortho* to the strongest electron-donating group.[14] Nucleophilic aromatic substitution, on the other hand, requires electron-deficient arenes with halogens and nitro groups as nucleofuges.[15] For cases in which regioselectivity issues may arise, such as the presence of multiple halogenated sites on an aromatic system, the Handy method was developed to designate the most electrophilic carbon of a halogenated heterocycle using ^{1}H NMR shifts of the corresponding dehalogenated analogues.[16]

This photoredox-catalyzed system possesses characteristics of both types of polar aromatic substitution: 1) electron-rich arenes undergo functionalization (E_AS) and 2) exogenous nucleophiles add to an electrophilic arene intermediate (S_NAr). However, since predictions of reactivity for E_AS and S_NAr rely on the reactivity of a neutral arene, we hypothesized that they would be inappropriate for predicting site selectivity with a transient arene cation radical intermediate.[18]

Arene cation radical intermediates are most commonly understood as delocalized in both charge and spin density. In some cases, however, a localized distonic cation radical is a more accurate representation. Determination of the spin density distribution by computational methods can lend insight into where the radicophilic character is localized on the cation radical intermediate. For example, prior calculations demonstrate that the spin density for the indole cation radical exists primarily at the 3-position, suggesting that the positive charge is shared between the nitrogen and the 2-position of the adjacent carbon atom.[22] These data indicate that distonic iminium radical intermediates can be generated through SET from arenes, provided that there is sufficient enamine character present in the neutral substrate. Similarly, for substrates such as benzofurans possessing enol ether character, we hypothesized that an oxocarbenium radical is likely the best description of the corresponding cation radical.

Studies by Fukuzumi and Yoshida have demonstrated the utility of computational methods to explain regioselectivity for a few select examples of aryl bromination[12] and amination reactions,[19] respectively, that proceed via cation radicals. However, both of these reports focused on simple benzenoid substrates. Based on prior art by Fukuzumi, we anticipated that the aryl carbon possessing the greatest difference in natural population analysis (NPA)[20] values between the cation radical and neutral species would be the most electrophilic and therefore the most probable site of functionalization as the cation radical. Consequently, we wondered whether this approach could be exploited on more complex aromatic and heteroaromatic systems utilized in systems previously studied in our laboratory.

We elected to employ the natural population analysis of both the cation radical and the neutral arene with calculations performed at the B3LYP/6-31G+(d,p) level of theory.[21] For anisole, the greatest difference in NPA values is at the position *para* to the methoxy substituent (Figure 2), which was confirmed experimentally (*vide infra*). While this approach cannot be extended to predicting reaction efficiency or regioisomeric ratios, we anticipated that it could be used as a tool to predict the primary site of reactivity.

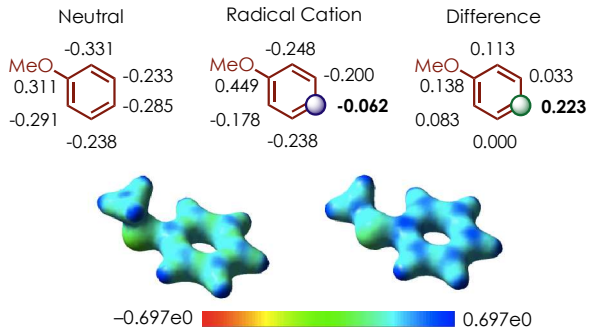

Figure 2. Anisole natural population analysis (NPA) values and electrostatic potential maps

While the aforementioned methods can be employed to determine the most likely site of aromatic C–H functionalization for arene cation radicals, determining the likelihood of the reactivity of a given aromatic system is less straightforward. Accordingly, we hypothesized that the likelihood of C–H functionalization in cation radical-mediated reactions might be determined from the difference between the cation radical and neutral arene NPA values. We hypothesized that a significant change in electron density between the neutral molecule and the cation radical is necessary for reactivity.

Aromatic Classes

To expand the scope and utility of these methodologies, we aimed to determine whether aromatic cores commonly used in pharmaceutical development could undergo functionalization. A variety of aromatic motifs were reactive using our methodology, which we decided to group into two main classes based on structural similarities: 1) six-membered aromatics, and 2) aromatics containing at least one five-membered heteroaromatic ring or aromatic bicyclic [4.3.0] core. The substrate classes that fall under the first category are benzenoids, pyridines, and quinolines. Benzenoids are ubiquitous in natural products and pharmaceuticals and have been extensively applied in the development of new drugs.[24] Pyridines and quinolines are among the most prevalent aromatic ring and nitrogen containing heterocycles found in U.S. FDA approved pharmaceuticals[25,26] and the latter is also present in several natural products including the cinchona alkaloids. The second category of heteroarenes include pyrazoles,[27,28]

indazoles,[29] bridging nitrogen polyaromatics,[30–38] benzofurans,[39] indoles,[40–42] and benzazoles[43–45] that have found wide application in drug discovery and incorporated in pharmaceuticals for a variety of indications.

Reaction Design

For many of the substrates reported in our previous communications, we were able to determine the number of regioisomers formed via GC-MS analysis. For most arenes, crude ^{1}H NMR spectra could be used to determine the selectivities. To extend this work to other heterocycles, we employed similar conditions as previously reported, the only difference being the use of an air atmosphere instead of pure O_2 as these conditions provided cleaner crude reaction mixtures, especially for substrates containing alkyl substituents. For some substrate classes, additional heating was required to observe productive C–N bond formation (see SI for details). We chose to utilize pyrazole as the nucleophile in this study since C–N bond formation at either nitrogen is inconsequential *vis a vis* regioselectivity. For arene substrates that afford the desired C–H functionalization adduct or gave only modest yields, we generally observed unreacted starting materials as the remainder of the mass balance.

RESULTS AND DISCUSSION

Six-Membered Aromatics

Benzenoids

In order to explore the reactivity of benzenoids toward C–H amination under photoredox catalysis, we selected substrates with a representative set of sterics and electronics that might be found in a range of potential substrates. For mono-substituted benzenes sufficiently electron-rich to be oxidized by the acridinium photocatalyst, we observed that in all cases, the *para* product was favored along with minor amounts of the *ortho* adduct (Figure 3). From the computational NPA values, the *para* position of mono-substituted arene cation radicals is predicted to be the most electrophilic position (see SI Table 1). Phenolic ether substrates (**2a-2e**) and biphenyl (**2f**) underwent functionalization at the *para* position as anticipated. Upon examination of benzenoids with two or more substituents, halide-functionalized arenes were compatible, as demonstrated by 2-chloroanisole (**2g**) and 3-bromoanisole (**2h**) and most importantly, did not act as nucleofuges as is the case in S_NAr chemistry or commonly in transition metal-catalyzed arene C–H functionalization. Experimentally, only one regioisomer was observed and in both cases, functionalization occurred *para* to the methoxy group, matching the computationally determined greatest difference in NPA charge between the cation radical and neutral compound. Despite the fact that 2-chloro-2'-methoxy-1,1'-biphenyl (**2i**) has eight distinct sites that could undergo functionalization, only one regioisomer was observed (**3i**). The site of functionalization matched the computational predictions, occurring on the more electron-rich ring *para* to the methoxy group and demonstrating that site selectivity between multiple arenes could be achieved. While a different set of anaerobic reaction conditions are required for alkyl-substituted arenes due to the formation of byproducts arising from benzylic oxidation, the site of functionalization for mesitylene (**2j**) and *m*-xylene (**2k**) was still predicted by the calculated NPA values (see SI Table 2). Urea **2l** and dihydrocoumarin **2m** underwent selective amination *para*- to the heteroatom, again in agreement with the largest NPA value difference.

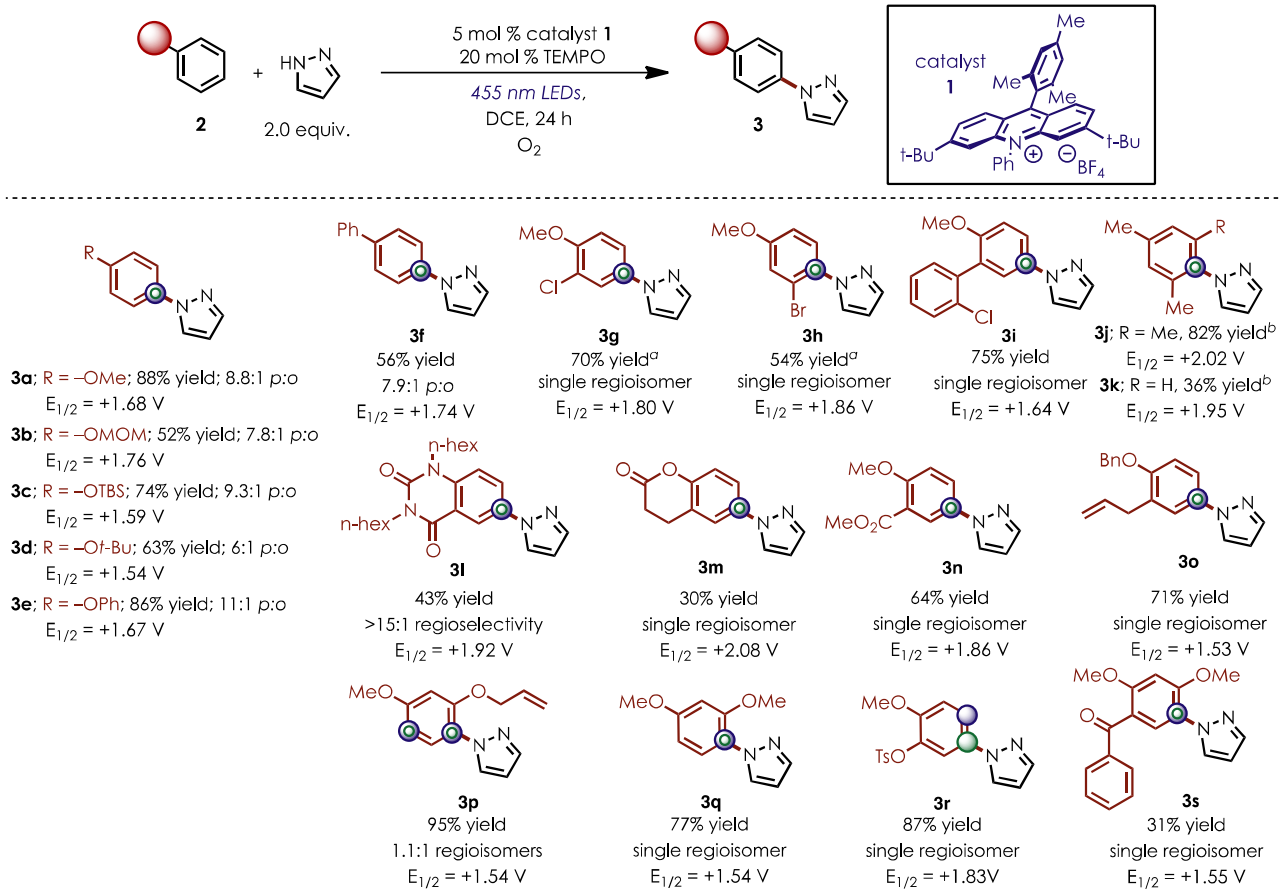

Figure 3. Benzenoid scope with predictions of site selectivity. Ratios refer to para:ortho (*p:o*) selectivity for the given isomer. Reactions were run in 1,2-dichloroethane (DCE) at 0.1 M concentration with respect to the arene limiting reagent. Computational results are highlighted using ● to show the site of most positive radical cation charge density, ● to show the largest NPA difference site and ◎ to show sites where the most positive radical cation charge density and largest NPA difference match. Redox potentials are all computationally determined and are calculated vs. SCE in MeCN. [a]Reaction run for 48 hours [b]Reaction run under N_2 with 1 equiv. of TEMPO

In addition to these substrates from our prior amination report, we wanted to demonstrate that additional benzenoid compounds from our arene cyanation work[11] participated in the amination chemistry to expand the functional group tolerance of the reaction. Esters were compatible (**2n**), as well as *O*-benzyl phenols (**2o**) and allyl substituents (**2o** and **2p**), even under aerobic conditions. Furthermore, single regioisomers were formed using 1,3-dimethoxybenzene (**2q**) and *O*-tosyl guaiacol (**2r**) in high yields. Trisubstituted arenes were also viable substrates for the C–H amination reaction, and compound **3s** was obtained in 31% yield as a single regioisomer with complete chemoselectivity for the more electron-rich arene. For all benzenoid substrates, experimental selectivity matched the computationally predicted site of largest NPA value difference (see SI Tables 1–3).

Pyridines

Unsubstituted pyridine has a calculated redox potential of $E_{calc,ox}$ (pyridine$^{\bullet+}$/pyridine) = +2.64 V vs SCE,[17] therefore, generation of the pyridinyl cation radical from relatively electron-poor pyridines using an acridinium photooxidant is unfavorable. However, when electron-donating groups were present, the oxidation potential was sufficiently lowered to allow for single electron oxidation by the photooxidant (see SI Table 4). As previously reported,[10] 2,6-dimethoxypyridine underwent amination to deliver a single regioisomer (**5a**) at the computationally predicted site (Figure 4). Surprisingly, 2,4-dimethoxypyridine afforded two products, **5b** and **5c**, in a 2.3:1 ratio, where the minor product **5c** results from reaction at the site with the greatest difference in NPA values. In this case, the major product of functionalization is not at the site of the largest NPA value difference due to the steric repulsion of the two methoxy substituents with the relatively bulky pyrazole nucleophile. 3,5-Dimethoxypyridine afforded the adduct **5d** as a single regioisomer in good yields, also matching the computational predictions. Additionally, a methoxy substituent could be replaced by a methyl group without diminishing reactivity. We observed desired reactivity with 2-methyl-6-methoxypyridine, but in order to avoid oxidation of the benzylic methyl group, anaerobic conditions were required. Computational predictions indicated a preference for functionalizing at the 3-position, and amination occurred at both the 3 and 5 positions, giving **5e** and **5f**, respectively. Overall, pyridines can be functionalized if they possess electron-donating substituents that attenuate the redox potential to values ≤ +2.15 V and generally undergo amination at the site with the largest difference in NPA values between the cation radical and neutral states.

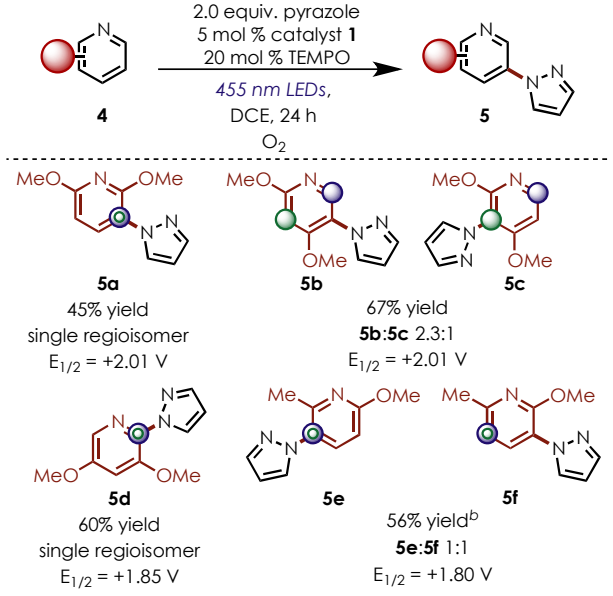

Figure 4. Pyridine scope with predictions of site selectivity. Reactions were run in 1,2-dichloroethane (DCE) at 0.1 M concentration with respect to the arene limiting reagent. Computational results are highlighted using ● to show the site of most positive radical cation charge density, ● to show the largest NPA difference site and ● to show sites where the most positive radical cation charge density and largest NPA difference match. Redox potentials are all computationally determined and are calculated vs. SCE in MeCN. [a]Reaction run under air instead of O_2 [b]Reaction run under N_2 with 1.0 equiv. of TEMPO.

Quinolines

Previously, we demonstrated that 6-methoxyquinoline provided a single regioisomer **7a** (Figure 5). For several additional quinoline substrates (**7b-7d**), we were able to predict the site of functionalization based on NPA differences between the cation radical and neutral state (see SI Table 5). For substrates such as 4-bromo-7-methoxyquinoline (**6e**), no desired product was formed, in accordance with the observation that there was no significant difference in the NPA values. In most cases, when there was a sufficient difference in NPA values, good yields and single regioisomers were observed. Unlike several other classes of heterocycles (*vide infra*), a specific position on the quinoline is not generally favored; instead, functionalization is highly dependent on the position of electron-donating substituents. For some examples such as 2-methyl-4-chloro-7-methoxyquinoline, **7d** was isolated as the major product, while *ipso* substitution of the –OMe group was observed as a minor product. In general, quinolines with a sufficiently large NPA difference underwent functionalization with site selectivity that reflected the computational prediction.

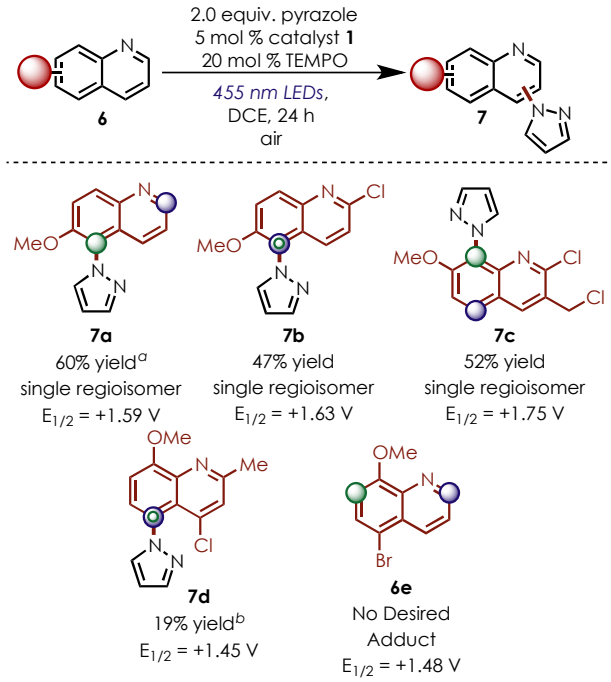

Figure 5. Quinoline scope with predictions of site selectivity. Reactions were run in 1,2-dichloroethane (DCE) at 0.1 M concentration with respect to the arene limiting reagent. Computational results are highlighted using ● to show the site of most positive radical cation charge density, ● to show the largest NPA difference site and ● to show sites where the most positive radical cation charge density and largest NPA difference match. Redox potentials are all computationally determined and are calculated vs. SCE in MeCN. [a]Reaction run under O_2 instead of air. [b]Ipso substitution at the methoxy observed.

In general, for six-membered aromatic systems, site selectivity matched what would be expected for electrophilic aromatic substitution,[14] despite the clear differences in operative mechanism. While the predictive model is needed to provide a theoretical basis for understanding the site selectivity, it is convenient to apply the same rules for E_AS to predict the regioselectivity for simple benzenoid C–H functionalization in these systems.

Aromatics Containing at Least One Five-Membered Ring

We anticipated that divergent reactivity might be observed between this class of heterocycles and six-membered aromatic rings due to the presence of enamine character in some of these systems. Heteroarenes such as pyrazoles and indoles participate in E_AS reactions in which the enamine character dictates the site of nucleophilic reactivity. While this innate enamine nucleophilicity is observed in some five-membered containing heterocycles, others such as indazoles or benzoxazoles are incapable of adopting enamine-like resonance structures. Previously, our lab has disclosed numerous examples of anti-Markovnikov alkene functionalization reactions using acridinium photoredox catalysts,[46] and we recognized that arenes with enamine character could also be treated as cyclic alkenes, from which a distonic iminium radical is resultant. With the knowledge that some five-membered ring containing heterocycles have a similar regioselectivity as enamines as the neutral arene, we wondered whether reactivity in this system would occur at the E_AS position similarly to the six-membered ring classes or if it would be more similar to a distonic iminium radical.

Pyrazoles

Pyrazole and *N*-methyl pyrazole (**8a**) are not sufficiently electron-rich to be oxidized by the photocatalyst, but with the addition of a methyl substituent such as with 1,3- and 1,4-dimethyl pyrazole, the redox potentials fall to $E_{calc,ox}$ (pyrazole^{+}/pyrazole) = +2.01 and +1.83 V vs SCE, respectively (Figure 6). Indeed, functionalization of these two substrates occurs in our system, favoring amination at the 5-position (**9b** and **9c**), which is the most electrophilic site of the cation radical (see SI Table 6).

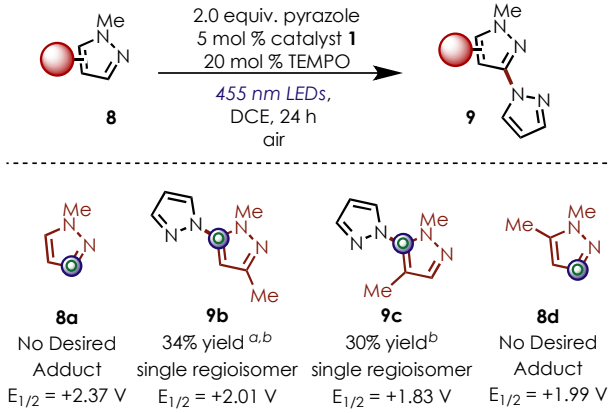

Figure 6. Pyrazole scope with predictions of site selectivity. Reactions were run in 1,2-dichloroethane (DCE) at 0.1 M concentration with respect to the arene limiting reagent. Computational results are highlighted using ● to show the site of most positive radical cation charge density, ● to show the largest NPA difference site and ● to show sites where the most positive radical cation charge density and largest NPA difference match. Redox potentials are all computationally determined and are calculated vs. SCE in MeCN. [a]Reaction run under O_2 instead of air. [b]^{1}H NMR yield with hexamethyldisiloxane internal standard.

When the methyl group is located at the 5-position, as with 1,5-dimethyl pyrazole, no functionalization occurred (**8d**). Thus, aryl functionalization of *N*-substituted pyrazoles occurs at the 5-position unless it is blocked, in which case no reactivity is observed.

Based on the trends observed with benzenoids, pyridines, and quinolines, if E_AS reactivity were used to predict site selectivity on pyrazoles, functionalization at the 4-position would be anticipated.[47,48] However, pyrazoles deviate from this trend, with *N*-methylpyrazoles reacting at the 5-position, likely due to the transient cation radical intermediate behaving as a distonic iminium radical instead of a delocalized arene cation radical. For this reason, **8d** is not functionalized due to the iminium position bearing the 5-methyl substituent. Thus, instead of drawing analogy to E_AS reactivity, pyrazoles can best be treated as cyclic iminium radicals to determine site selectivity.

Indazoles

We previously disclosed that *N*-methylindazole functionalizes at the 3-position (Figure 7, **11a**), which matches the computationally calculated site of the largest NPA charge difference (see SI Table 7). Reactivity was also observed with 7-bromo-*N*-methylindazole, affording predominantly the 3-functionalized product, **11b**, along with minor regioisomer **11c** at the 4-position. This matches the largest NPA difference being at the 3-position, however, the NPA differences at both the 3- and 4-positions are very similar, correlating to productive C–N bond formation observed at both sites. We observe accurate predictions for the site selectivity of major and minor regioisomers with the model, although quantitative analysis of the relative amounts of products formed is beyond the scope of the computations. No amination occurs when the 3-position is substituted, as in 3-bromoindazole (**10d**), possibly due to steric hindrance at both the 4- and 7-positions with the bulky pyrazole nucleophile.

Although they are fused pyrazole heterocycles, indazoles do not possess the enamine character highlighted above for pyrazoles. For the indazoles that were studied, the model predicted and we observed functionalization at the same site as one would anticipate for E_AS.[27,48]

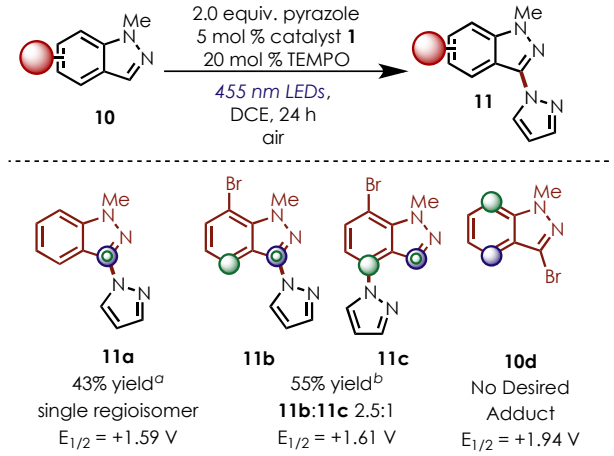

Figure 7. Indazole scope with predictions of site selectivity. Reactions were run in 1,2-dichloroethane (DCE) at 0.1 M concentration with respect to the arene limiting reagent. Computational results are highlighted using ● to show the site of most positive radical cation charge density, ● to show the largest NPA difference site and ● to show sites where the most positive radical cation charge density and largest NPA difference match. Redox potentials are all computationally determined and are calculated vs. SCE in MeCN. [a]Reaction run under O_2 instead of air. [b]^{1}H NMR yield with hexamethyldisiloxane internal standard.

Bridging Nitrogen Polyaromatic Systems

Computational predictions demonstrated that many bridging nitrogen polyaromatic compounds such as imidazopyrimidines, imidazopyridazines and pyrazolopyrimidines should be susceptible to oxidation by the photocatalyst (see SI Table 8) which was verified experimentally and in most cases, only one regioisomer was observed. Imidazo[1,2-*b*]pyridazines afforded products **13a**–**13d** with functionalization exclusively at the 3-position regardless of the substituents (Figure 8). A more electron-deficient imidazo[1,2-*b*]pyridazine **12d** showed a significant decrease in yield and despite the fact that two halogen substituents were present, functionalization still occurred at the 3-position. For imidazo[1,2-*a*]pyrimidine, only one regioisomer (**13e**) was formed in good yield, matching the predicted site of functionalization at the 3-position. For imidazo[1,2-*b*]pyridazines and imidazo[1,2-*a*]pyrimidines, enamine character is present in the ring system. Similarly to *N*-methylpyrazoles, reactivity of these bridging nitrogen polyaromatic systems occurs at the electrophilic carbon of the iminium radical.

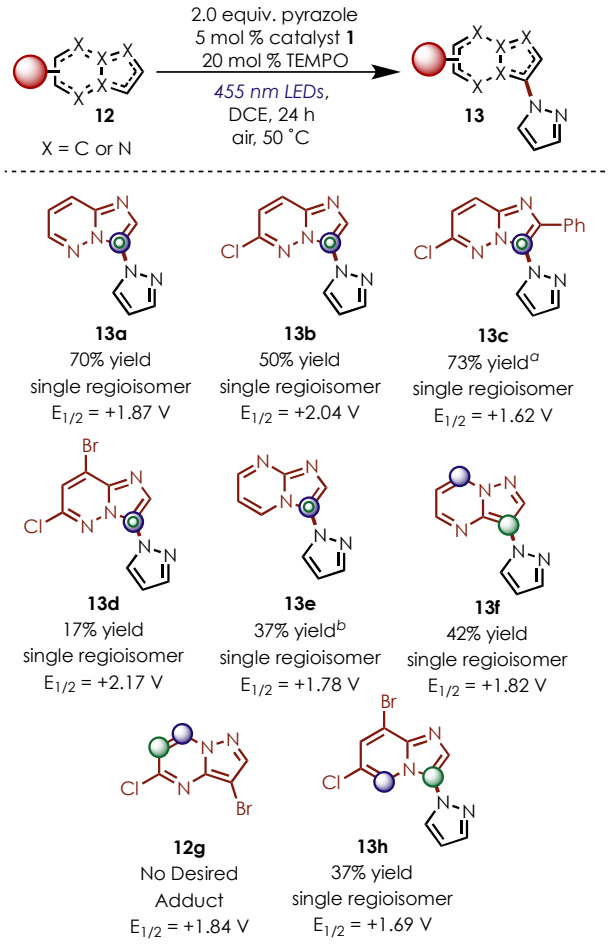

Figure 8. Bridging nitrogen polyaromatic heterocycle scope with predictions of site selectivity. Reactions were run in 1,2-dichloroethane (DCE) at 0.1 M concentration with respect to the arene limiting reagent. Computational results are highlighted using ● to show the site of most positive radical cation charge density, ● to show the largest NPA difference site and ● to show sites where the most positive radical cation charge density and largest NPA difference match. Redox potentials are all computationally determined and are calculated vs. SCE in MeCN. [a]Reaction run at room temperature under O_2 [b]^{1}H NMR yield with hexamethyldisiloxane internal standard.

Undecorated pyrazolo[1,5-*a*]pyrimidine produced adduct **13f** in 42% yield, also undergoing functionalization at the 3-position. Since this substrate cannot generate an iminium cation radical that is unsubstituted at the electrophilic position, its reactivity cannot be discussed in this way. Rather, selectivity in this case is what would be expected for E_AS reactivity. Substrate classes such as the pyrazolo[1,5-a]pyrimidine, for which enamine character is present but does not describe the site of functionalization, highlight the advantage of the predictive model, which indeed anticipates the observed regioselectivity. Halogenated pyrazolo[1,5-*a*]pyrimidines were not reactive under these conditions and in the case of **12g**, none of the expected adduct was observed. Based on the computational model, the difference in NPA values between the neutral molecule and the arene cation radical was insignificant, likely resulting in the lack of reactivity. However, halogens could be tolerated on the imidazo[1,2-*a*]pyridine core to afford **13h** in a 37% yield, in agreement with the site of the greatest NPA difference. The site of functionalization also correlates to the electrophilic site of the iminium radical that is generated after SET. For many bridging nitrogen polyaromatic systems, SET from the enamine dictates site selectivity, which matches the computational predictions for the most electrophilic site. Even for substrates in which the enamine reactivity is nontrivial to describe qualitatively, the predictive model provides a simple strategy for determining site selectivity.

Benzofurans and Indoles

Unsubstituted benzofuran (**14a**) affords a complex mixture of products under the reaction conditions, and the amination product was never isolated (Figure 9). However, addition of a methoxy substituent at either the 5 or 7 position afforded the aryl amination products in modest yields (**15b**-**15d**). Intriguingly, 5-methoxybenzofuran was functionalized to give **15b** and **15c** – the amination product and a difunctionalization product – in a 1.2:1 ratio. With the addition of a substituent at the 2-position, as in 2-methyl-5-methoxybenzofuran, only difunctionalized product **15e** was observed in 36% yield. Benzofurans undergo C–H functionalization at the most electropositive site of the cation radical instead of the position with the largest NPA difference (see SI Table 9), and in some cases, difunctionalization of the substrate was observed. If benzofuran were treated as a cyclic enol ether, SET would lead to a distonic oxocarbenium radical, nucleophilic addition to which would afford the products functionalized at the 2-position. In the cases where difunctionalization is observed, the benzylic radical resulting from nucleophilic addition to the oxocarbenium can be oxidized to the carbocation, which is susceptible to addition of a second equivalent of nucleophile. While this heterocycle class does not follow the prediction that reactivity occurs at the site bearing the largest NPA difference, it still follows that the site with oxocarbenium character is the most electrophilic position.

Indole afforded no amination product under the reaction conditions, but very little starting material was recovered due to significant unidentified byproduct formation. By contrast, when the indole bore a methyl substituent, desired reactivity was observed, albeit in low yields (Figure 9). Further optimization for this class of heterocycles is needed to achieve synthetically viable yields, but selectivity was determined and matched the computational prediction (see SI Table 9). When the methyl group is at the 2-position of the indole (**14f**), no reaction is observed, and starting material is returned, but the inclusion of methyl substituents on the six-membered ring facilitates reactivity. Treating indoles in a similar fashion to benzofurans, these cyclic enamines undergo SET to generate a distonic iminium radical. In the case of 2-methylindole, addition

to the 2-position is possible but highly reversible, resulting in returned starting material. In cases where a methyl substituent is present but not located at the 2-position, addition of the amine nucleophile is favored at the 2-position (**15g** and **15h**). In contrast to the majority of the aforementioned heteroaromatic systems, amination occurs at the most electrophilic site of the cation radical instead of the site of the largest NPA difference. Nucleophilic addition at the 2-position results in a more stable benzylic radical intermediate, leading to the observed regioselectivity.

Neither benzofurans nor indoles undergo functionalization at the site of largest NPA difference, where the model predicts reactivity. Compared to other arenes studied, benzofurans and indoles possess significantly less aromatic character.[49,50] Accordingly, we propose that they not be treated as aromatic compounds for the purpose of this model and should instead be considered to react as electron-rich styrene derivatives. Based on this premise, functionalization at the 2-position forms the stabilized benzylic radical intermediate. If these classes were sufficiently aromatic to justify their treatment as such in the model, rearomatization of the benzylic radical would outcompete oxidation and subsequent difunctionalization but difunctionalization can be sometimes be observed. Since benzofurans and indoles deviate from other aromatic compounds in this way, it is more appropriate to interpret their reactivity as that of a distonic cation radical arising from alkene oxidation rather than that of a delocalized arene cation radical.

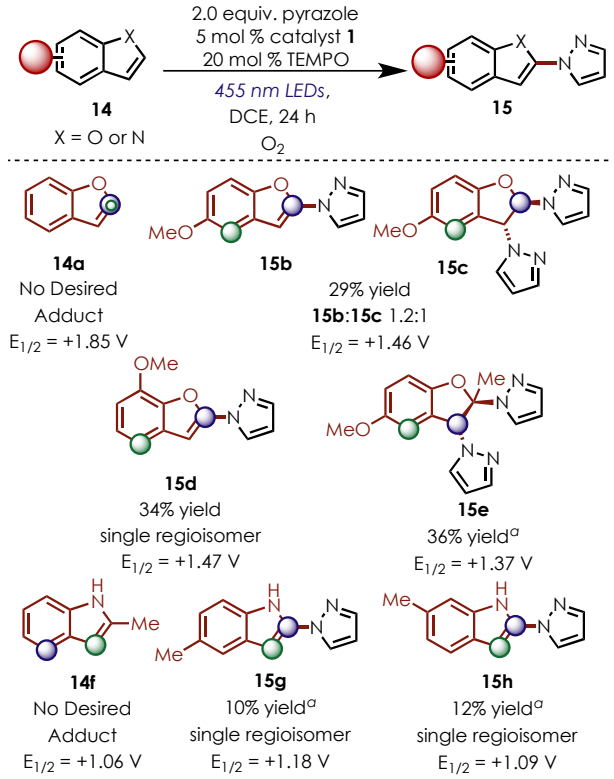

Figure 9. Benzofuran and indole scope with predictions of site selectivity. Reactions were run in 1,2-dichloroethane (DCE) at 0.1 M concentration with respect to the arene limiting reagent. Computational results are highlighted using ● to show the site of most positive radical cation charge density, ● to show the largest NPA difference site and ● to show sites where the most positive radical cation charge density and largest NPA difference match. Redox potentials are all computationally determined and are calculated vs. SCE in MeCN. [a]Reaction run under air.

Benzazoles

While the scope of this article does not address every commonly used aromatic heterocycle, we demonstrate the wide variety of electron-rich arenes that can undergo amination in the photoredox catalytic system. With 2-methylbenzoxazole (Figure 10), the major product **17a** matches the largest NPA difference site (see SI Table 10). Benzothiazoles were shown to react to form **17b** and **17c** in modest yields in better than 10:1 selectivity for the products shown. Finally, 2-chloro-*N*-methylbenzimidazole provided two products in a 3:1 ratio and modest yield (**17d** and **17e**). Again, the predictive model accurately foretold the major products of these heterocycles based on the largest NPA difference. The sites of functionalization for benzazoles correlate well with E_AS site selectivity,[51,52] similarly to the six-membered aromatic compounds discussed previously. Though the computational model was needed to understand the origins of site selectivity, the analogy to E_AS regioselectivity can be used as a strategy to predict site selectivity in many cases.

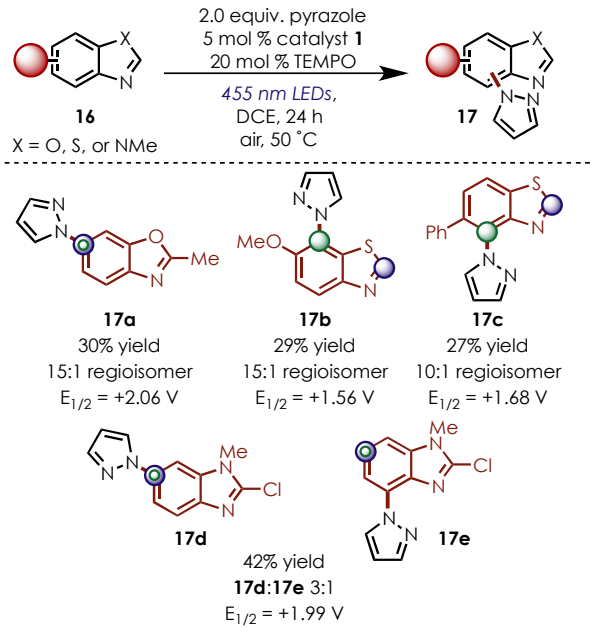

Figure 10. Benzazoles with predictions of site selectivity. Reactions were run in 1,2-dichloroethane (DCE) at 0.1 M concentration with respect to the arene limiting reagent. Computational results are highlighted using ● to show the site of most positive radical cation charge density, ● to show the largest NPA difference site and ● to show sites where the most positive radical cation charge density and largest NPA difference match. Redox potentials are all computationally determined and are calculated vs. SCE in MeCN.

Other Nucleophiles

While the use of pyrazole demonstrates the general reactivity and selectivity with a variety of aromatic coupling partners, we also wanted to investigate the regioselectivity with respect to other nucleophiles (Figure 11). Additional nitrogen nucleophiles added to the most electrophilic site on a variety of heterocycles (see SI Tables 4–10). In our prior work, we were able to add an ammonia equivalent to electron-rich arenes, giving functionalization at the site of the largest NPA difference (**18a** and **18b**). Site selectivities observed when a variety of other azole nucleophiles were used (**18c-18g**) matched those reported above when using pyridines, quinolines, pyrazoles, indazoles, and benzofurans with pyrazole as the coupling partner. We also wanted to test whether other aryl functionalization reactions such as the C–H cyanation[11]

developed in our laboratory followed similar site selectivities (**18h** and **18i**). The results in Figure 11 demonstrate that other nucleophiles exhibit the same site selectivities for a variety of heterocyclic classes as previously discussed, allowing the predictive model to be generalized to include a range of nucleophiles.

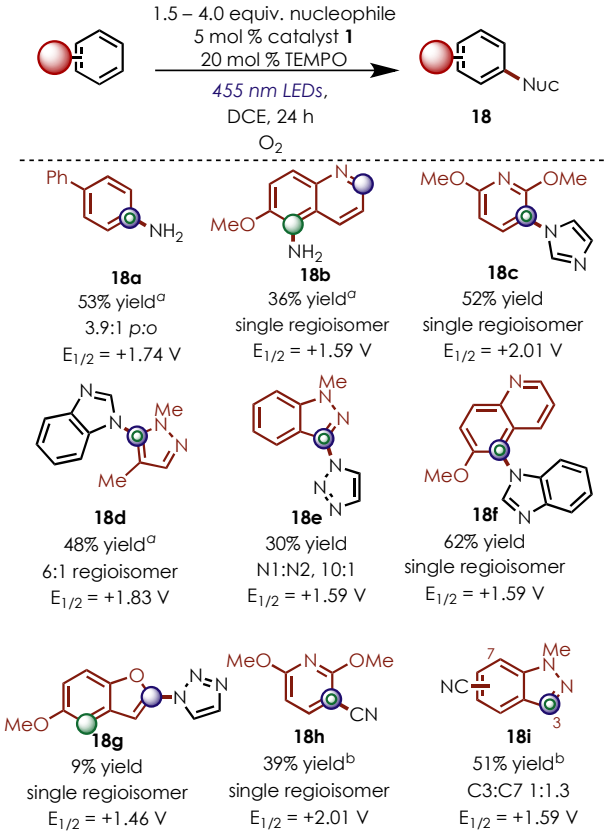

Figure 11. Additional nucleophile scope with predictions of site selectivity. Reactions were run in 1,2-dichloroethane (DCE) at 0.1 M concentration with respect to the arene limiting reagent. Computational results are highlighted using ● to show the site of most positive radical cation charge density, ● to show the largest NPA difference site and ● to show sites where the most positive radical cation charge density and largest NPA difference match. Redox potentials are all computationally determined and are calculated vs. SCE in MeCN. [a]$NH_4CO_2NH_2$ (4.0 equiv), 5 mol % catalyst **1**, 20 mol % TEMPO, 10:1 DCE:H_2O, O_2, 24 h. [b]TMSCN (1.5 equiv), 5 mol % catalyst **1**, 10:1 MeCN:pH 9 buffer, O_2, 24 h.

Complex Structures

The utility of this photoredox-catalyzed C–H functionalization strategy can be further underscored in the application to late stage functionalizations of complex substrates (Figure 12). As we previously disclosed, quinine, naproxen and capsaicin derivatives all underwent regioselective amination (**19a-19c**), and the experimental findings again matched the site with the largest NPA difference (see SI Table 11). Functionalization of gemfibrozil methyl ester afforded the pyrazole functionalized product **19d** in a 32% yield as a single regioisomer. Both pyrazole and cyanide added to the same position on gemfibrozil (**19d** and **19e**), matching the site with the largest difference in NPA values. Cyanide also added to Boc-melatonin at the site with the largest NPA value difference (**19f**). This deviates from previously discussed *N*–H indoles because the carbamate protection disfavors iminium radical formation. For all of these complex, late stage functionalization targets, we observe reactivity at sites similar to the parent heterocycles. The application of the aryl amination and cyanation chemistries to late stage functionalization demonstrates the advantage of the predictive model for determining site selectivity.

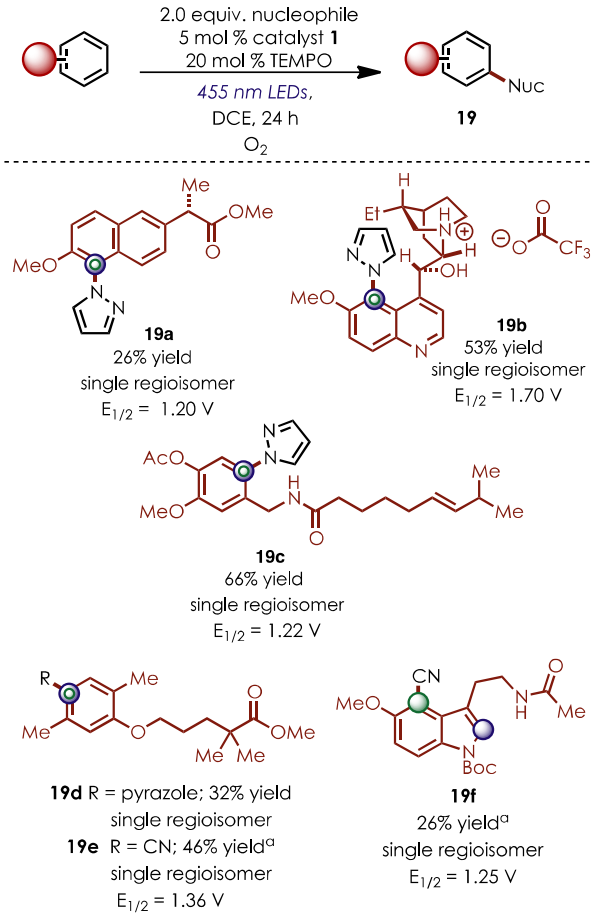

Figure 12. Complex arene scope with predictions of site selectivity. Reactions were run in 1,2-dichloroethane (DCE) at 0.1 M concentration with respect to the arene limiting reagent. Computational results are highlighted using ● to show the site of most positive radical cation charge density, ● to show the largest NPA difference site and ● to show sites where the most positive radical cation charge density and largest NPA difference match. Redox potentials are all computationally determined and are calculated vs. SCE in MeCN. [a]TMSCN (1.5 equiv), 5 mol % catalyst **1**, 10:1 MeCN:pH 9 buffer, O_2, 24 h.

CONCLUSIONS

As shown with these numerous examples, the arene C–H functionalization strategy can be applied to a wide variety of biologically active heterocyclic cores and even in more complex compounds in late stage applications.

In an attempt to generalize the reactivity and site selectivity observed as a function of benzenoid and heterocycle class, we have summarized our findings in Figures 13 and 14. Two general classifications can be used to distinguish between substrate groups: 1) the site of functionalization matches E_AS selectivity (Figure 13, Part A); 2) the site of functionalization matches where iminium or oxocarbenium radical character predominates (Figure 13, Part B). Overall, substituted benzenoids, pyridines, and quinolines undergo reactivity directed by the most electron-releasing group, similarly to E_AS selectivity (Figure 14). Indazoles generally react at the 3-position, unless it is blocked, which leads to an unreactive substrate, and benzazoles that are unsubstituted on the 6-membered ring generally undergo functionalization *para* to the nitrogen substituent. For these classes, the use of simple E_AS selectivity rules can be used to predict the site of

functionalization more rapidly and is supported by our computational model.

N-alkylated pyrazoles give rise to reactivity at the 5-position, the electrophilic site of the iminium radical, except when that site bears a substituent, in which case they are unreactive. Bridging nitrogen polyaromatic compounds react similarly, highlighting the predictable reactivity of the iminium radicals. Benzofurans and indoles generally react at the 2-position, the site with oxocarbenium or iminium character, unless substitution is present at that location. While benzofurans and indoles are aromatic systems, for the purpose of this model, treating them as cyclic alkenes is a more appropriate depiction. It should be stressed that these are not meant to be absolute rules, but rather, rough guidelines of when and where to anticipate reactivity on heteroaromatic systems.

As mentioned in part (i) of the predictive model, an arene must be sufficiently electron-rich to undergo SET to the acridinium photoredox catalyst, as determined by oxidation potentials. Several classes of aromatic heterocycles we studied were generally too electron-deficient for the acridinium catalyst to oxidize, including pyrimidines, pyridazines, pyrazines, purines, and nucleobases (Figure 13, part C). Since these heterocycles are unreactive under the reaction conditions, selective functionalization of more electron-rich aromatics could be possible with these heteroarene classes. We anticipate that the knowledge of reactivity and selectivity obtained through this predictive model will allow for these methodologies to find wide application in late-stage functionalization of biologically active compounds.

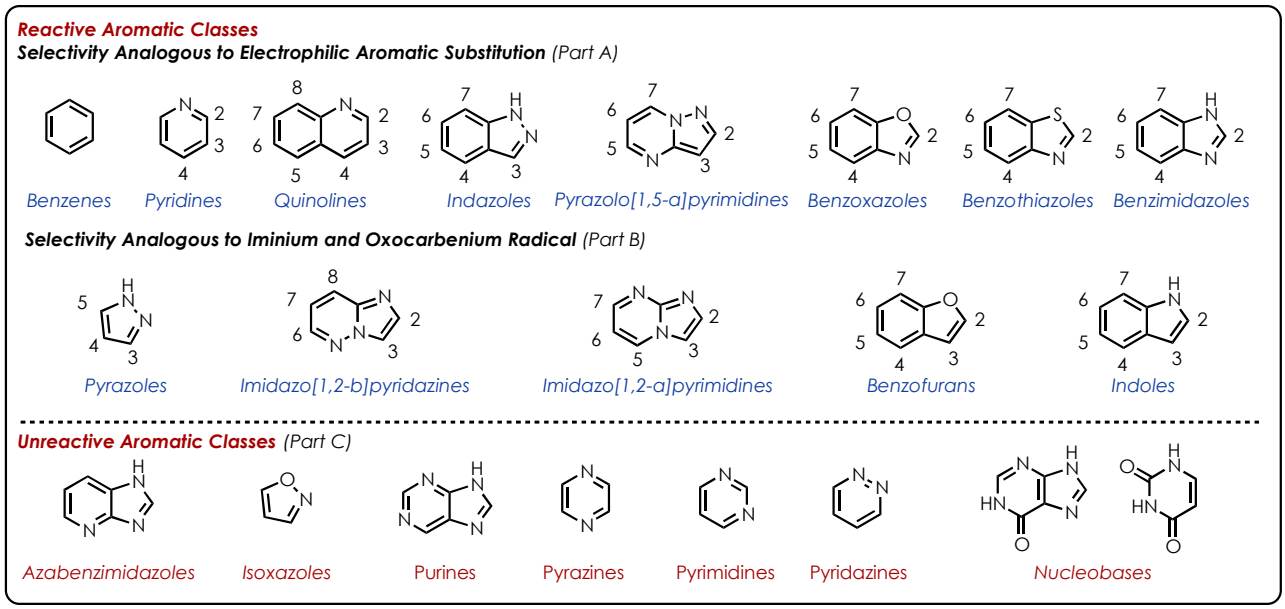

Figure 13. Chart describing reactivity patterns for heterocycle classes.

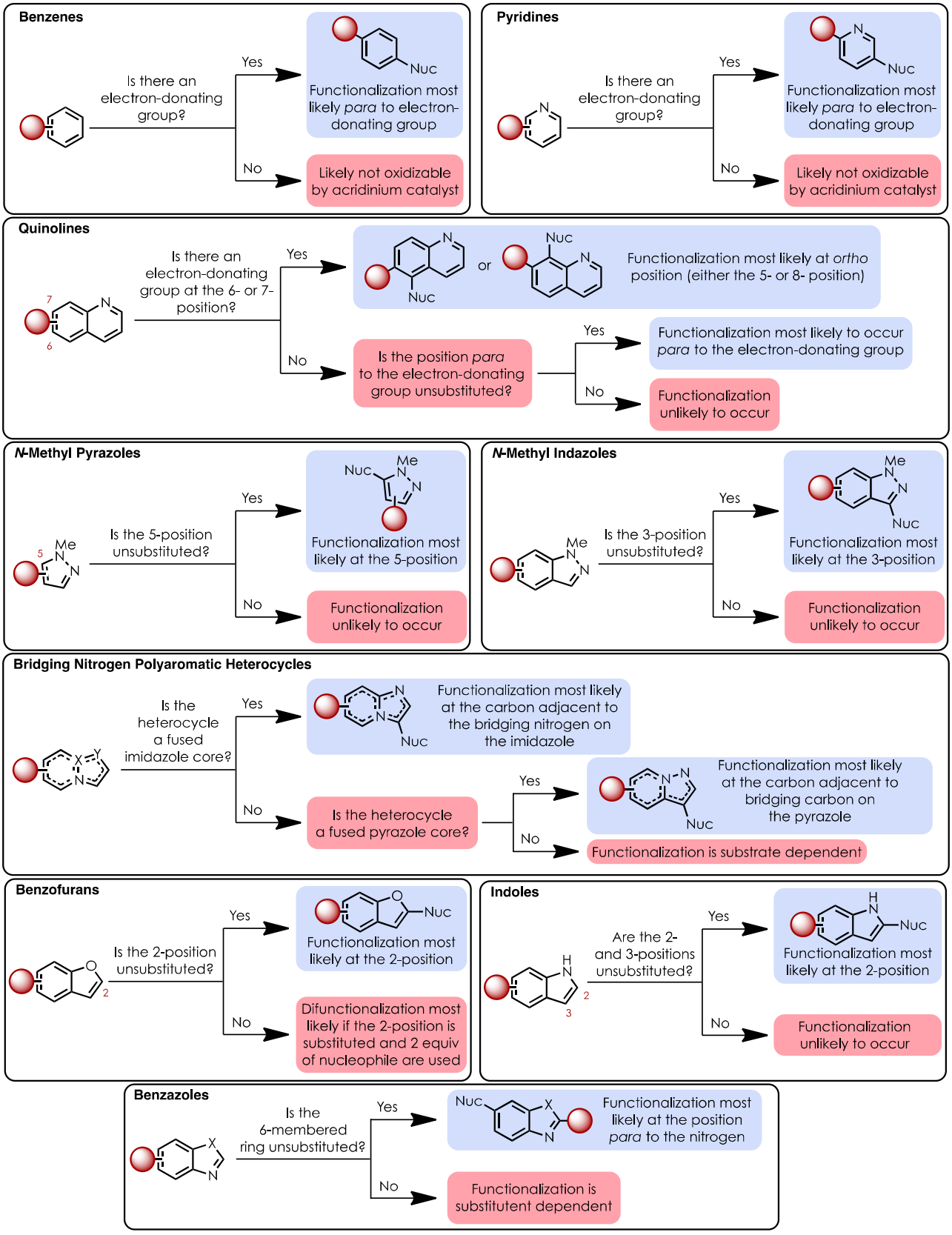

Figure 14. Flow chart describing general selectivities for heterocycles grouped by class.

AUTHOR INFORMATION

Corresponding Author

nicewicz@unc.edu

Funding Sources

No competing financial interests have been declared.

ACKNOWLEDGEMENT

This work was supported by the National Institutes of Health (NIGMS) Award No. R01 GM120186. The authors would like to thank Pete Delgado and Melissa Orlando for supplying the acridinium photocatalyst. Thomas Dice, Ritesh Tichkule, and Jonathan Grob are acknowledged for helping with the automated lab equipment. Matthew Daniels and Dr. Kian Tan are acknowledged for discussions on photoredox catalysis. KAM and DN would like to thank Novartis for sponsoring a mini-sabbatical for KAM and providing reagents for this work. We thank the University of North Carolina's Department of Chemistry Mass Spectrometry Core Laboratory for its assistance with mass spectrometry analysis. We would also like to thank the reviewers for their insightful comments on an earlier version of this paper.

ASSOCIATED CONTENT

Supporting Information

The Supporting Information is available free of charge on the ACS Publications website at http://pubs.acs.org.

Experimental procedures, spectral data and computational results for all new compounds (PDF)

REFERENCES

(1) Cernak, T.; Dykstra, K. D.; Tyagarajan, S.; Vachal, P.; Krska, S. W. *Chem Soc Rev* **2016**, *45*, 546–576.
(2) Dai, H.-X.; Stepan, A. F.; Plummer, M. S.; Zhang, Y.-H.; Yu, J.-Q. *J. Am. Chem. Soc.* **2011**, *133*, 7222–7228.
(3) Neufeldt, S. R.; Sanford, M. S. *Acc. Chem. Res.* **2012**, *45*, 936–946.
(4) Bigi, M.; Liu, P.; Zou, L.; Houk, K.; White, M. *Synlett* **2012**, *23*, 2768–2772.
(5) Bess, E. N.; Bischoff, A. J.; Sigman, M. S. *Proc. Natl. Acad. Sci.* **2014**, *111*, 14698–14703.
(6) Bess, E. N.; DeLuca, R. J.; Tindall, D. J.; Oderinde, M. S.; Roizen, J. L.; Du Bois, J.; Sigman, M. S. *J. Am. Chem. Soc.* **2014**, *136*, 5783–5789.
(7) Gormisky, P. E.; White, M. C. *J. Am. Chem. Soc.* **2013**, *135*, 14052–14055.
(8) O'Hara, F.; Blackmond, D. G.; Baran, P. S. *J. Am. Chem. Soc.* **2013**, *135*, 12122–12134.
(9) Bess, E. N.; Guptill, D. M.; Davies, H. M. L.; Sigman, M. S. *Chem Sci* **2015**, *6*, 3057–3062.
(10) Romero, N. A.; Margrey, K. A.; Tay, N. E.; Nicewicz, D. A. *Science* **2015**, *349*, 1326–1330.
(11) McManus, J. B.; Nicewicz, D. A. *J. Am. Chem. Soc.* **2017**.
(12) Ohkubo, K.; Mizushima, K.; Iwata, R.; Fukuzumi, S. *Chem. Sci.* **2011**, *2*, 715.
(13) Ohkubo, K.; Fujimoto, A.; Fukuzumi, S. *J. Phys. Chem. A* **2013**, *117*, 10719–10725.
(14) Taylor, R. J. Wiley: Electrophilic Aromatic Substitution Chichester, West Sussex, England ; New York, 1990.
(15) Bunnett, J. F.; Zahler, R. E. *Chem. Rev.* **1951**, *49*, 273–412.
(16) Handy, S. T.; Zhang, Y. *Chem Commun* **2006**, 299–301.
(17) Roth, H.; Romero, N.; Nicewicz, D. *Synlett* **2016**, *27*, 714–723.
(18) Schmittel, M.; Burghart, A. *Angew. Chem. Int. Ed. Engl.* **1997**, *36*, 2550–2589.
(19) Morofuji, T.; Shimizu, A.; Yoshida, J. *J. Am. Chem. Soc.* **2013**, *135*, 5000–5003.
(20) Reed, A. E.; Weinstock, R. B.; Weinhold, F. *J. Chem. Phys.* **1985**, *83*, 735–746.
(21) Computations were carried out using the Gaussian 09 software package (Frisch, M. J.; et al. Gaussian 09, revision D.01; Gaussian, Inc.: Wallingford, CT, 2009). See Supporting Information for additional details and the full citation for Gaussian 09.
(22) Walden, S. E.; Wheeler, R. A. *J. Phys. Chem.* **1996**, *100*, 1530–1535.
(23) Saito, I.; Matsugo, S.; Matsuura, T. *J. Am. Chem. Soc.* **1979**, *101*, 7332–7338.
(24) Taylor, R. D.; MacCoss, M.; Lawson, A. D. G. *J. Med. Chem.* **2014**, *57*, 5845–5859.
(25) Vitaku, E.; Smith, D. T.; Njardarson, J. T. *J. Med. Chem.* **2014**, *57*, 10257–10274.
(26) Prajapati, S. M.; Patel, K. D.; Vekariya, R. H.; Panchal, S. N.; Patel, H. D. *RSC Adv.* **2014**, *4*, 24463.
(27) Song, S.; Sun, X.; Li, X.; Yuan, Y.; Jiao, N. *Org. Lett.* **2015**, *17*, 2886–2889.
(28) Khan, M. F.; Alam, M. M.; Verma, G.; Akhtar, W.; Akhter, M.; Shaquiquzzaman, M. *Eur. J. Med. Chem.* **2016**, *120*, 170–201.
(29) Wada, Y.; Shirahashi, H.; Iwanami, T.; Ogawa, M.; Nakano, S.; Morimoto, A.; Kasahara, K.; Tanaka, E.; Takada, Y.; Ohashi, S.; *et al. J. Med. Chem.* **2015**, *58*, 6048–6057.
(30) Byth, K. F.; Cooper, N.; Culshaw, J. D.; Heaton, D. W.; Oakes, S. E.; Minshull, C. A.; Norman, R. A.; Pauptit, R. A.; Tucker, J. A.; Breed, J.; Pannifer, A.; Roswell, S,; Stanway, J. J.; Valentine, A. L.; Thomas, A. P. *Bioorg. Med. Chem. Lett.* **2004**, *14*, 2249–2252.
(31) Choi, H.-S.; Rucker, P. V.; Wang, Z.; Fan, Y.; Albaugh, P.; Chopiuk, G.; Gessier, F.; Sun, F.; Adrian, F.; Liu, G.; Hood, T.; Li, N.; Jia, Y.; Che, J.; McCormack, S.; Li, A.; Li, J.; Steffy, A.; Culazzo, A.; Tompkins, C.; Phung, V.; Kreusch, A.; Lu, M.; Hu, B.; Chaudhary, A.; Prashad, M.; Tuntland, T.; Liu, B.; Harris, J.; Seidel, H. M.; Loren, J.; Molteni, V. *ACS Med. Chem. Lett.* **2015**, *6*, 562–567.
(32) Chen, X.; Xu, W.; Wang, K.; Mo, M.; Zhang, W.; Du, L.; Yuan, X.; Xu, Y.; Wang, Y.; Shen, J. *J. Med. Chem.* **2015**, *58*, 8529–8541.
(33) O'Connor, S. P.; Wang, Y.; Simpkins, L. M.; Brigance, R. P.; Meng, W.; Wang, A.; Kirby, M. S.; Weigelt, C. A.; Hamann, L. G. *Bioorg. Med. Chem. Lett.* **2010**, *20*, 6273–6276.
(34) Venkatesan, A. M.; Dehnhardt, C. M.; Chen, Z.; Santos, E. D.; Dos Santos, O.; Bursavich, M.; Gilbert, A. M.; Ellingboe, J. W.; Ayral-Kaloustian, S.; Khafizova, G.; Brooijmans, N.; Mallon, R.; Hollander, I.; Feldberg, L.; Lucas, J.; Yu, K.; Gibbons, J.; Abraham, R.; Mansour, T. S. *Bioorg. Med. Chem. Lett.* **2010**, *20*, 653–656.
(35) Elie, R.; Rüther, E.; Farr, I.; Emilien, G.; Salinas, E. *J. Clin. Psychiatry* **1999**, *60*, 536–544.
(36) Xu, Y.; Brenning, B. G.; Kultgen, S. G.; Foulks, J. M.; Clifford, A.; Lai, S.; Chan, A.; Merx, S.; McCullar, M. V.; Kanner, S. B.; Han, K.-K. *ACS Med. Chem. Lett.* **2015**, *6*, 63–67.
(37) Enguehard-Gueiffier, C.; Gueiffier, A. *Mini-Rev. Med. Chem.* **2007**, *7*, 888–899.
(38) Cheng, Y.; Moraski, G. C.; Cramer, J.; Miller, M. J.; Schorey, J. S. *PLoS ONE* **2014**, *9*, e87483.
(39) Asif, M. *J. Anal. Pharm. Res.* **2016**, *3*.
(40) Ishikura, M.; Abe, T.; Choshi, T.; Hibino, S. *Nat. Prod. Rep.* **2013**, *30*, 694.
(41) de Sa Alves, F.; Barreiro, E.; Manssour Fraga, C. *Mini-Rev. Med. Chem.* **2009**, *9*, 782–793.
(42) Sravanthi, T. V.; Manju, S. L. *Eur. J. Pharm. Sci.* **2016**, *91*, 1–10.

(43) Demmer, C. S.; Bunch, L. *Eur. J. Med. Chem.* **2015**, *97*, 778–785.
(44) Prajapati, N. P.; Vekariya, R. H.; Borad, M. A.; Patel, H. D. *RSC Adv* **2014**, *4*, 60176–60208.
(45) Bansal, Y.; Silakari, O. *Bioorg. Med. Chem.* **2012**, *20*, 6208–6236.
(46) Margrey, K. A.; Nicewicz, D. A. *Acc. Chem. Res.* **2016**, *49*, 1997–2006.
(47) Zhao, Z.; Wang, Z. *Synth. Commun.* **2007**, *37*, 137–147.
(48) Rodriguez, R. A.; Pan, C.-M.; Yabe, Y.; Kawamata, Y.; Eastgate, M. D.; Baran, P. S. *J. Am. Chem. Soc.* **2014**, *136*, 6908–6911.
(49) Balaban, A. T.; Oniciu, D. C.; Katritzky, A. R. *Chem. Rev.* **2004**, *104*, 2777–2812.
(50) Palmer, M. H.; Kennedy, S. M. F. *J. Chem. Soc. Perkin Trans. 2* **1974**, 1893.
(51) Kihel, A. E.; Benchidmi, M.; Essassi, E. M.; Danion-Bougot, R. *Synth. Commun.* **1999**, *29*, 387–397.
(52) Ward, E. R.; Poesche, W. H. *J. Chem. Soc. Resumed* **1961**, 2825.

Table of Contents Graphic